PHOTONICS Research

# Hybrid level anharmonicity and interference-induced photon blockade in a two-qubit cavity QED system with dipole–dipole interaction

C. J. Zhu,[1,2,3] K. Hou,[1,4] Y. P. Yang,[1,6] and L. Deng[5,7]

[1]MOE Key Laboratory of Advanced Micro-Structured Materials, School of Physics Science and Engineering, Tongji University, Shanghai 200092, China
[2]School of Physical Science and Technology, Soochow University, Suzhou 215006, China
[3]Collaborative Innovation Center of Light Manipulations and Applications, Shandong Normal University, Jinan 250358, China
[4]Department of Mathematics and Physics, Anhui Jianzhu University, Hefei 230601, China
[5]Center for Optics Research and Engineering (CORE), Shandong University, Qingdao 266237, China
[6]e-mail: yang_yaping@tongji.edu.cn
[7]e-mail: lu.deng@email.sdu.edu.cn

Received 29 January 2021; revised 11 April 2021; accepted 4 May 2021; posted 4 May 2021 (Doc. ID 421234); published 21 June 2021

**We theoretically study a quantum destructive interference (QDI)-induced photon blockade in a two-qubit driven cavity quantum electrodynamics system with dipole–dipole interaction (DDI). In the absence of dipole–dipole interaction, we show that a QDI-induced photon blockade can be achieved only when the qubit resonance frequency is different from the cavity mode frequency. When DDI is introduced the condition for this photon blockade is strongly dependent upon the pump field frequency, and yet is insensitive to the qubit–cavity coupling strength. Using this tunability feature we show that the conventional energy-level-anharmonicity-induced photon blockade and this DDI-based QDI-induced photon blockade can be combined together, resulting in a hybrid system with substantially improved mean photon number and second-order correlation function. Our proposal provides a nonconventional and experimentally feasible platform for generating single photons.** 

https://doi.org/10.1364/PRJ.421234

## 1. INTRODUCTION

Nonclassical states of light have properties that challenge the usual notions of classical physics. These states not only show fundamental differences between quantum and classical physics, but also allow scientists to test the validity of quantum mechanics experimentally. Besides fundamental physics considerations, nonclassical states of light play an essential role in quantum information protocols such as quantum key distributions [1], quantum cryptography [2], quantum entanglement [3], and optical quantum computing [4]. Moreover, certain types of nonclassical states have reduced fluctuations compared to classical states, which may lead to improvements in the field of precision measurements [5–7].

Photon blockade (PB) is an important technique for generating nonclassical light. So far, two physical schemes have been used to achieve a strong PB effect. The conventional photon blockade (CPB) scheme is based on the well-known eigenenergy-level anharmonicity (ELA) in cavity quantum electrodynamics (QED) [2,8]. When a photon is tuned to resonantly excite the atom–cavity QED system from its ground state to the states of the lowest doublet, the absorption of a second photon at the same frequency is blockaded because transitions to higher doublets are significantly off-resonance because of ELA [9]. Consequently, antibunching photons with sub-Poissonian statistical characteristics can be generated. In the strong coupling regime, where the coupling between the quantum emitter and the cavity is larger than the cavity decay rate, this ELA-based CPB has been experimentally and theoretically studied in various quantum systems [9–14], including atom–cavity QED [15–17], optomechanical systems [18–20], circuit QED systems [21–23], Kerr-nonlinearity systems [24–26], and so on.

An unconventional photon blockade (UCPB) relies on the quantum destructive interference (QDI) between two different quantum transition pathways from the ground state to a two-photon excited state. Liew and Savona first proposed the concept of QDI-based UCPB [27,28] via weak nonlinearities, opening more degrees of freedom for operation. Although both CPB and UCPB result in strong antibunched photons, the underlying physical mechanisms are completely different. The reduction of the two-photon state is achieved by a destructive interference in UCPB rather than the nonlinearity of the dressed spectrum in the strong coupling regime. Since strong

coupling condition is not required for achieving QDI-based UCPB [29], this scheme has received great attention and it has been proposed for many quantum systems including quantum dots [30], third-order nonlinearity scheme [31,32], optical parametric amplifier scheme [33], optomechanical device [34–36], non-Markovian system [37], two-emitter-cavity [38], and Jaynes–Cummings model [39–42]. Recently, the QDI-induced PB has been demonstrated in superconducting QED systems [43,44]. It must be noted that single-atom UCPB effect can only be achieved in a cavity-driven system, not an atom-driven system [42].

In this work, we propose a two-qubit (e.g., two-level atoms) single-cavity system to study a hybrid PB effect in which an ELA-based mechanism and a QDI-based mechanism act cooperatively. The central enabler of this atom-driven hybrid PB is the inter-atom ("super-qubit") dipole–dipole interaction (DDI). In this configuration a two-qubit system is coherently "locked" by a cavity mode, effectively making it a super-qubit system with two "internal" excitation pathways. Here, each pathway involves one qubit in a coherently locked and driven two-qubit-one-cavity system. This new scheme mimics the four-level diamond excitation scheme in nonlinear optics [45] where robust QDI effect can play a dominant role [46] and we shall refer it as a diamond PB (DPB). We find that the excitation pathways via two individual but locked qubits are indistinct when the qubit resonance frequency is the same as that of the cavity mode, yielding a constructive interference. However, when the qubit resonance frequency is shifted from the cavity mode frequency, the two excitation pathways become distinct, yielding a destructive interference. Unlike UPBs where the field–cavity coupling strength is essential in the destructive interference formed by different excitation pathways in the same single qubit, the DPB scheme described here is independent of coupling strength. This implies that in the presence of DDI both the ELA and QDI can induce PB operations at the same probe field coupling strength. This opens the possibility for an extremely strong PB effect that yields a well-detectable mean photon number, the virtual of an ELA-PB, and yet an extremely small $g^{(2)}(0)$, which is the pinnacle of a QDI-PB.

## 2. MODEL SYSTEM

We consider two identical two-level qubits (two-level atom) with resonant frequency $\omega_a$ located in a single-mode cavity having resonant frequency $\omega_c$. The ground (excited) atomic state is labeled as $|g\rangle$ ($|e\rangle$) and the positions of two qubits are given by $\mathbf{x}_j$ ($j = 1,2$) (Fig. 1). The two qubits are coherently driven by a pump field with angular frequency $\omega_p$ and Rabi frequency $\Omega_p$. The DDI with strength $J$ plays a key role to the statistical properties of the cavity field when $d = |\mathbf{x}_1 - \mathbf{x}_2| < \lambda_a \equiv 2\pi c/\omega_a$. Assuming that these two qubits have the same qubit–cavity coupling strength $g$ and using rotating wave approximation, the Hamiltonian in the presence of DDI can be expressed as

$$H = \sum_{j=1}^{2} -\Delta_a \sigma_j^\dagger \sigma_j - \Delta_c a^\dagger a + \sum_{j=1}^{2} g(a^\dagger \sigma_j + a\sigma_j^\dagger) + J(\sigma_1 \sigma_2^\dagger + \sigma_2 \sigma_1^\dagger) + \sum_{j=1}^{2} \Omega_p(\sigma_j + \sigma_j^\dagger), \quad (1)$$

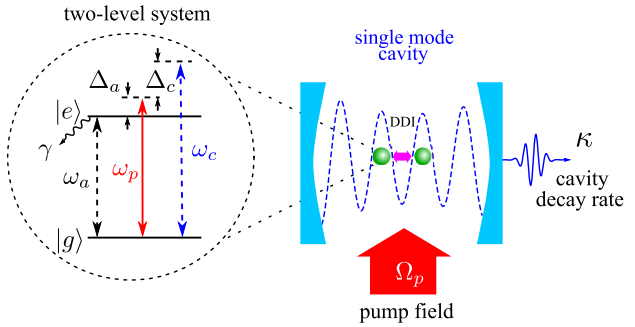


**Fig. 1.** Sketch of the two-qubit cavity QED system with different cavity mode frequency $\omega_c$ and qubit resonant frequency $\omega_a$. A pump field $\Omega_p$ couples the qubit ground state $|g\rangle$ and excited state $|e\rangle$ with the angular frequency $\omega_p$. $\gamma$ and $\kappa$ denote the qubit decay rate and the cavity decay rate, respectively. Here, DDI represents the dipole–dipole interaction when two qubits are close enough.

where $\Delta_c = \omega_p - \omega_c$ and $\Delta_a = \omega_p - \omega_a$ are the cavity and qubit frequency detunings, respectively. Here, $a$ ($a^\dagger$) is the cavity field annihilation (creation) operator, and $\sigma_j = |g\rangle_j\langle e|$ is the lowering operator of the $j$th qubit.

The dynamics of this two-qubit coherently driven system is described by the master equation [47]:

$$\frac{\partial \rho}{\partial t} = -i[H,\rho] + \mathcal{L}_\kappa[\rho] + \mathcal{L}_\gamma[\rho] + \mathcal{L}_{\gamma'}[\rho], \quad (2)$$

where $\rho$ is the system density matrix, $\mathcal{L}_\kappa[\rho] = 0.5\kappa(2a\rho a^\dagger - a^\dagger a\rho - \rho a^\dagger a)$ describes the cavity leakage with rate $\kappa$, and $\mathcal{L}_\gamma[\rho] = \sum_{j=1}^{2} 0.5\gamma(2\sigma_j\rho\sigma_j^\dagger - \sigma_j^\dagger\sigma_j\rho - \rho\sigma_j^\dagger\sigma_j)$ indicates free-space damping of the $j$th qubit with rate $\gamma$. The last term $\mathcal{L}_{\gamma'}[\rho] = 0.5\gamma' \sum_{i\neq j}(2\sigma_i\rho\sigma_j^\dagger - \sigma_i^\dagger\sigma_j\rho - \rho\sigma_i^\dagger\sigma_j)$ describes the collective damping resulting from the mutual exchange of spontaneously emitted photons through a common reservoir. Under the condition of $J \gg \gamma'$, the last term in Eq. (2) can be safely neglected as treated in Rydberg atoms [48–50].

## 3. ELA AND QDI-INDUCED PBS IN THE ABSENCE OF DDI

We first consider the case where the DDI is absent, i.e., two qubits are well separated with $k_a d \gg 1$ ($k_a = 2\pi/\lambda_a$). In this case, using collective states, i.e., $|gg,n\rangle$, $|\pm,n\rangle \equiv (|eg,n\rangle + |ge,n\rangle)/\sqrt{2}$, and $|ee,n\rangle$, one can rewrite the Hamiltonian [Eq. (1)] to give $H = \Delta_a S^\dagger S + \Delta_c a^\dagger a + 2g(aS^\dagger + a^\dagger S) + \Omega_p(S + S^\dagger)$ with collective operator $S = (\sigma_1 + \sigma_2)/\sqrt{2}$. In the strong coupling regime, it is convenient to describe the system by using the dressed state representation [see Fig. 2(a) and Appendix A.1]. In $n$-photon space the eigenstates form ladder-type doublets with unevenly separated energy levels. When the pump field was tuned to one of the states of the lowest doublet, i.e., $\Psi_1^{(\pm)}$ with the condition of $2g^2 = \Delta_a\Delta_c$, the absorption of a second photon of the pump field will be blocked due to the large energy mismatch resulting from energy-level anharmonicity.

To show this feature, we calculate the second-order correlation function $g^{(2)}(0) = \langle a^\dagger a^\dagger a a\rangle/(\langle a^\dagger a\rangle)^2$ by numerically solving the master equation. With system parameters $\Delta_c = -30\kappa$, $g = 5\kappa$, $\gamma = \kappa$, and $\Omega_p = 0.1\kappa$, Fig. 2(c) shows two PBs

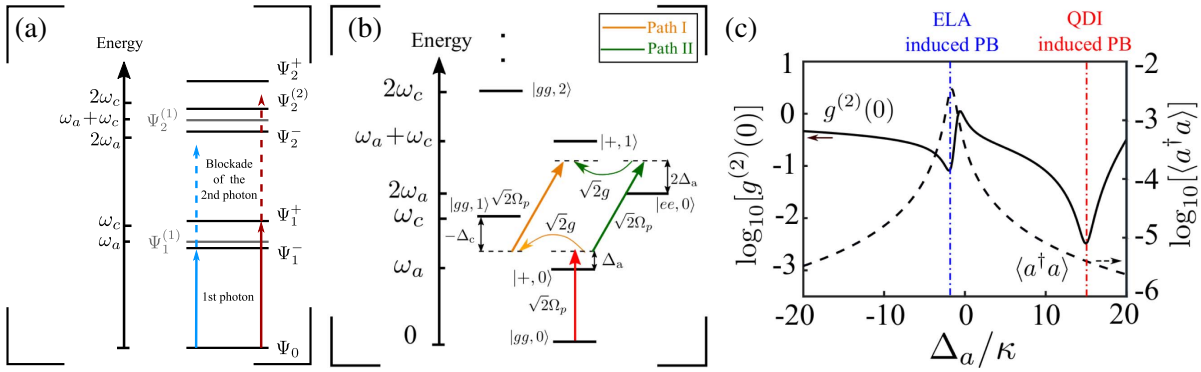


**Fig. 2.** (a), (b) The anharmonic ladder-type energy structure and the destructive interference pathways for the ELA-based and QDI-induced PBs, respectively. In (a), the absorption of a second photon of the pump field will be blocked due to the large energy mismatch if the pump field is tuned to the state $\Psi_1^{(\pm)}$ as denoted by the blue and red arrows, respectively. In (b), two interference pathways from state $|+,0\rangle$ to state $|+,1\rangle$ are indicated by the yellow and green arrows, respectively. (c) The equal-time second-order correlation function $g^{(2)}(0)$ (solid curve) and mean photon number $\langle a^\dagger a\rangle$ (dashed curve) as a function of the normalized detuning $\Delta_a/\kappa$. Here, we chose $J=0$, $\Delta_c=-30\kappa$, $g=5\kappa$, $\gamma=\kappa$, and $\Omega_p=0.1\kappa$.

originated from different mechanisms. The blue dashed–dotted line indicates the detuning $\Delta_a\approx -1.6\kappa$ for realizing an ELA-induced PB operation as discussed above, whereas the red dashed–dotted line shows the location of the QDI-induced PB operation. The latter exhibits near 2 orders of magnitude smaller $g^{(2)}(0)$, a virtue of the QDI-based PB operation. However, the mean photon number only peaks at the location of ELA-based PB operation. The 3-order of magnitude difference in mean photon number demonstrates the significant experimental detection advantage of the ELA scheme over the QDI scheme.

The physical mechanism of the QDI-based PB can be explained by using the collective state picture. Figure 2(b) exhibits its two pathways for two-photon excitation of the state $|+,1\rangle$ after direct one-photon excitation of the state $|+,0\rangle$. One path is indicated by straight and curved yellow arrows representing $|+,0\rangle\overset{\sqrt{2}g}{\rightarrow}|gg,1\rangle\overset{\sqrt{2}\Omega_p}{\rightarrow}|+,1\rangle$ and the other path is indicated by straight and curved green arrows representing $|+,0\rangle\overset{\sqrt{2}\Omega_p}{\rightarrow}|ee,0\rangle\overset{\sqrt{2}g}{\rightarrow}|+,1\rangle$. When $\Delta_a=\Delta_c$, these two excitation pathways are indistinguishable so that the two-photon excitation can be enhanced due to the constructive interference. However, when $\Delta_a\neq\Delta_c$, these two excitation pathways are distinct and can lead to a destructive interference that blocks two-photon excitation of state $|+,1\rangle$. This is the essence of the QDI-induced PB effect. Using the amplitude equations, one can show that the condition for achieving this QDI-induced PB is $\Delta_c=-2\Delta_a$, which is independent of the coupling strength. This important feature implies that it is possible to shift and overlap, using a third cooperative interaction element, the peak QDI-PB operation regime to the optimum ELA-PB operation regime, creating a novel PB operation with large mean photon number and yet extremely small $g^{(2)}(0)$ [see discussion below and Appendix A.2 and A.3].

We note that such a quantum interference by excitation pathways does not exist in a single-qubit atom-driven QED system [42]. In the single-qubit case, the two-photon state $|g,2\rangle$ can only be excited via a single pathway, i.e., $|g,0\rangle\overset{\Omega_p}{\rightarrow}|e,0\rangle\overset{g}{\rightarrow}|g,1\rangle\overset{\Omega_p}{\rightarrow}|e,1\rangle\overset{g}{\rightarrow}|g,2\rangle$. This is the reason why without the assistance of extra nonlinearity single-atom QDI-based UCPB can only be realized in a cavity-driven system. We also note that the QDI-induced PB in the two-qubit QED system described in this work is different from those reported in the literature [28,43,44]. Most noticeably, the condition for realizing the QDI-induced DPB studied here is insensitive to the coupling strength and this indicates that the scheme is more robust and immune to field-related fluctuations in applications.

## 4. DIPOLE–DIPOLE INTERACTION INDUCED STRONG PB EFFECT

Figure 2(c) shows that the optimum operation regimes of the ELA scheme and the QDI scheme occur at different PB operational frequencies. We naturally ask if an additional interaction control mechanism can enable optimum performance of both regimes at a single PB operation frequency so that the advantages of both schemes can be realized simultaneously. As we show below, the DDI between two atoms can indeed achieve this goal, resulting in a hybrid PB that preserves the virtue of large mean photon number as well as the extremely small $g^{(2)}(0)$.

In the presence of DDI, the state $|+,n\rangle$ is shifted by an amount of $J$ which characterizes the DDI strength. Consequently, the condition for achieving ELA-induced PB becomes $2g^2=\Delta_c(\Delta_a-J)$. It can be shown that the condition for realizing the QDI-induced PB remains unchanged. This is because for the QDI-induced PB both $|+,0\rangle$ and $|+,1\rangle$ states are shifted by the same amount of $J$ in the same direction. It is this differential change that provides a tunability that enables the overlap of operational frequencies of both schemes. This desired operation regime can be achieved by making $\Delta_c=-2\Delta_a$ (green dashed line), resulting in a very strong PB phenomenon, as shown in Figs. 3(a) and 3(b). Here, an order of magnitude mean photon number increase and more than 4 orders of magnitude reduction of $g^{(2)}(0)$ are achieved simultaneously at the same PB operational frequency of $\Delta_a/\kappa=15$ with the DDI strength $J=\Delta_a+g^2/\Delta_a\approx 3.5g$

[black solid [in Fig. 3(a)] and dashed [in Fig. 3(b)] curves correspond to those shown in Fig. 2(c)].

Based on the relation $g^2 = -\Delta_a(\Delta_a - J)$, one can easily find the condition $J \geq 2g$ for obtaining the frequency to achieve this hybrid PB operation. In Fig. 4, we plot the second-order correlation function $\log_{10}[g^{(2)}(0)]$ [panel (a)] and the mean photon number $\log_{10}[\langle a^\dagger a\rangle]$ [panel (b)] as functions of the DDI strength $J/g$ and detuning $\Delta_a/\kappa$ by setting $\Delta_c = -2\Delta_a$ (other system parameters are the same as those used in Fig. 3). The condition for frequency-matched operation $g^2 = -\Delta_a(\Delta_a - J)$ is indicated by the dashed curves. Clearly, $J \geq 2g$ is a threshold for a PB operation with minimum $g^{(2)}(0)$.

Taking $J = 2g$ we show the influence of qubit–cavity coupling strength on the PB operation in Figs. 5(a) and 5(b). These are contour plots of $\log_{10}[g^{(2)}(0)]$ and $\log_{10}[\langle a^\dagger a\rangle]$ as functions of the normalized detuning $\Delta_a/\kappa$ and atom–cavity coupling strength $g/\kappa$ by taking $\Delta_c = -2\Delta_a$. The white dashed lines denote the optimal condition of PB operation, i.e., $g = \Delta_a$. With this optimal condition, the $g^{(2)}(0)$ of the PB can be improved by increasing the atom–cavity coupling strength [see Fig. 5(a)]. In Fig. 5(b) the mean photon number is always at its maximum but the parameter space for reaching this optimal number increases. It is worthy to point out that this scheme has a broad range of parameters to realize vanishingly small second-order correlation function, i.e., $g^{(2)}(0) < 0.01$. The minimum requirement for the qubit–cavity coupling strength is $g > \kappa$,

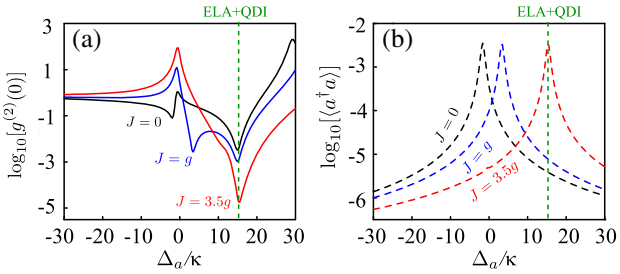


**Fig. 3.** Logarithmic plots of (a) the second-order correlation function $g^{(2)}(0)$ and (b) the mean photon number $\langle a^\dagger a\rangle$ as functions of the normalized detuning $\Delta_a/\kappa$ with the DDI strength $J = 0$ (black curves), $g$ (blue curves), and $3.5g$ (red curves), respectively. The green dashed line indicates the condition $\Delta_c = -2\Delta_a$. Other system parameters are the same as those used in Fig. 2(c).

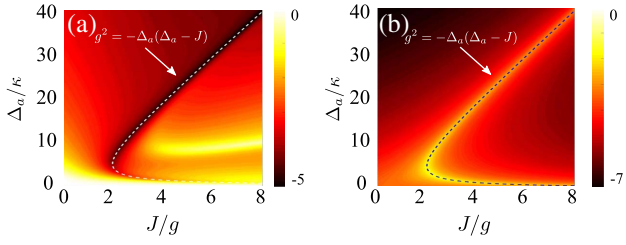


**Fig. 4.** Logarithmic plots of (a) the second-order correlation function $g^{(2)}(0)$ and (b) the mean photon number $\langle a^\dagger a\rangle$ as functions of the DDI strength $J/g$ and detuning $\Delta_a/\kappa$ by setting $\Delta_c = -2\Delta_a$ and $g = 5\kappa$. Other system parameters are the same as those used in Fig. 3. The dashed curves denote the optimal condition $g^2 = -\Delta_a(\Delta_a - J)$.

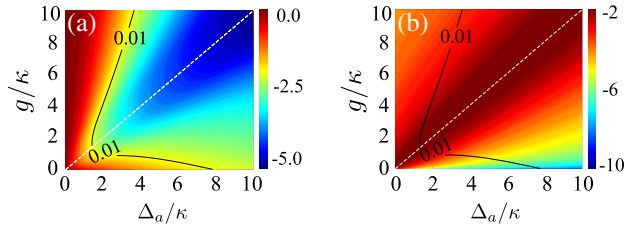


**Fig. 5.** Logarithmic plots of (a) the second-order correlation function $g^{(2)}(0)$ and (b) the mean photon number $\langle a^\dagger a\rangle$ against the detuning $\Delta_a/\kappa$ and coupling strength $g/\kappa$ with $\Delta_c = -2\Delta_a$ and $J = 2g$. The white dashed line corresponds to the condition $g = \Delta_a$, while the black solid curves denote $g^{(2)}(0) = 0.01$.

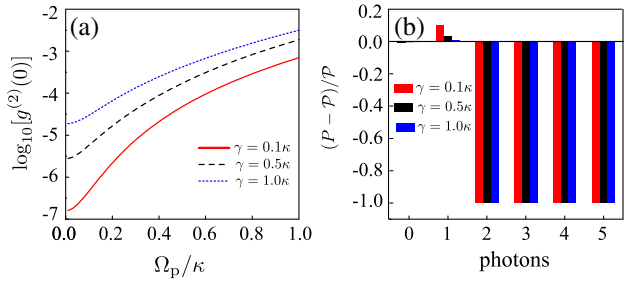


**Fig. 6.** (a) The second-order correlation function $\log_{10}[g^{(2)}(0)]$ versus the normalized pump field Rabi frequency $\Omega_p/\kappa$ with spontaneous decay rate $\gamma/2\pi = 0.1\kappa$ (red solid curves), $0.5\kappa$ (black dashed curves), and $\kappa$ (blue dotted curves), respectively. (b) The plot of the photon number in Fock states with $\Omega_p = 0.2\kappa$. Here, the system parameters are given by $g = 2\kappa$, and $J = \Delta_c = -2\Delta_a = 2g$.

indicated by the cross point of the black solid curve and white dashed line in Fig. 5.

Besides coupling strength, the atom driving field Rabi frequency and atomic decay rate also affect the PB effect. As shown in Fig. 6(a), although $g^{(2)}(0)$ increases as the driving field Rabi frequency $\Omega_p$ increases, strong PB phenomenon (defined as $g^{(2)} < 0.01$) still can be achieved with the DPB scheme. Moreover, the weaker the atomic spontaneous decay rate, the stronger the PB effect becomes. In Fig. 6(b), we show the quantum statistic properties of the cavity field by calculating the relative deviations of the cavity photon distribution $P(n)$ from the Poisson distribution $\mathcal{P}(n) \equiv \langle n\rangle^n e^{-\langle n\rangle}/n!$ with the same mean photon number $\langle n\rangle = \langle a^\dagger a\rangle$, i.e., $[P(n) - \mathcal{P}(n)]/\mathcal{P}(n)$. It is clear that the probability for detecting a single photon, i.e., $P(1)$ is greatly enhanced as the qubit decay rate decreases, but the probabilities for detecting $n \geq 2$ photons are strongly suppressed.

## 5. EXPERIMENTAL CONSIDERATIONS

The proposed two-qubit hybrid PB/DPB model may be realized by placing two quantum dots in an optical cavity/waveguide [51–53] or a superconductive microwave resonator with two Rydberg atoms [43,54–56]. With current experimental technology [57], the minimal condition of $J > 2g > 4\kappa$ can be satisfied if the distance between two quantum dots is much

smaller than the wavelength. For the latter case, large DDI can be realized using trapped cold Rydberg atoms [56,58–60]. Here, $^{87}$Rb atoms from a cold atom cloud trapped in a background magneto-optical trap can be employed to load an optical cavity. For a cloud that has a density of $10^{17}$ m$^{-3}$ two optical tweezers operating at 900 nm wavelength can be injected into the atom cloud laterally in a single-pass configuration. Using optics with a numerical aperture of ∼0.5, a tight focus of a few micrometers in diameter can be achieved and the trap centers can be controlled to have a separation of 10 μm by slight tilting the focusing optics [58,61]. The excitation to Rydberg state of $n = 60$–$90$ can be achieved using a combination of red and blue lasers via a two-photon step-up process. The cavity has a length of a few centimeters with a confocal parameter of the order of 10 μm, ensuring equal Rydberg atom excitation in the two near-by dipole traps. The advantage of the microwave scheme is that atom–atom interaction is not based on inter-atom DDI but on the common cavity mode. In essence, the cavity plays a triple role of level asymmetry, quantum interference, and atom–atom interaction whereas in the case of optical cavity the cavity plays a dual role of level asymmetry and quantum interference.

## 6. CONCLUSION

In summary, we have investigated a new photon blockade effect using an atom–atom dipole–dipole interaction assisted joint ELA- and QDI-scheme two-qubit QED system. In the absence of DDI, we show that optimal QDI-induced photon blockade can be realized only at qubit resonance frequency that is different from the cavity mode frequency and the PB operation mean photon number is low. We derived conditions for the ELA-based CPB and QDI-based UCPB, revealing that the condition for QDI-induced PB depends only on the pump field frequency and the PB effect is insensitive to the qubit–cavity coupling strength. This new joint ELA-QDI PB scheme with DDI as a mediator forms a highly effective hybrid diamond PB that exhibits a very strong PB effect, having more than an order of magnitude improvement on mean photon numbers and yet retaining the extremely low second-order correlation function. Our work provides a theoretical foundation for possible experimental demonstration of this diamond-scheme PB for highly efficient PB operation. The implementation of this protocol is potentially demonstrable using quantum systems such as a semiconductor quantum dot or quantum well cavity QED system [62,63], Rydberg atom–cavity QED system [64,65], and circuit cavity QED system [66]. It may lead to a new type of hybrid single-photon source for quantum information processing and communication.

## APPENDIX A

### 1. Condition of ELA-Based PB without DDI

We first consider the case where the DDI is absent. Neglecting the driving term (i.e., setting $\Omega_p = 0$), and using the collective states as basis $(|gg,n\rangle, |+,n-1\rangle, |-,n-1\rangle, |ee,n-2\rangle)$ with $|\pm\rangle = (|eg\rangle \pm |ge\rangle)/\sqrt{2}$, the Hamiltonian in the $n$-photon space can be expressed in the following matrix form:

$$H^{(n)} = \begin{pmatrix} n\omega_c & \sqrt{2n}g & 0 & 0 \\ \sqrt{2n}g & \omega_a + (n-1)\omega_c & 0 & \sqrt{2(n-1)}g \\ 0 & 0 & \omega_a + (n-1)\omega_c & 0 \\ 0 & \sqrt{2(n-1)}g & 0 & 2\omega_a + (n-2)\omega_c \end{pmatrix}. \tag{A1}$$

Specifically, in the one-photon space, the eigenvalues of the Hamiltonian $H^{(1)}$ can be solved analytically, which reads

$$E_1^{(1)} = \omega_a, \quad \text{with } \Psi_1^{(1)} = |-,0\rangle, \tag{A2a}$$

$$E_1^{(\pm)} = \frac{1}{2}\left[\omega_c + \omega_a \pm \sqrt{8g^2 + (\omega_a - \omega_c)^2}\right] \text{ with}$$

$$\Psi_1^{(\pm)} = N_1^{(\pm)}\left[-\frac{\omega_a - \omega_c \pm \sqrt{8g^2 + (\omega_a - \omega_c)^2}}{2g}|gg,1\rangle + |+,0\rangle\right], \tag{A2b}$$

where $N_1^{\pm}$ are the corresponding normalization constants. It can be clearly seen that the product state $|-,0\rangle$ is the dark state, which does not couple other states of the system.

The condition of the ELA-based PB can be obtained by setting $\omega_p = E_1^{(+)}$ or $\omega_p = E_1^{(-)}$. Thus, we can obtain

$$\Delta_a + \Delta_c = \sqrt{8g^2 + (\Delta_c - \Delta_a)^2}, \tag{A3}$$

by taking $\omega_p = E_1^{(+)}$, which can be further simplified as

$$g^2 = \frac{1}{2}\Delta_c\Delta_a. \tag{A4}$$

Likewise, one can obtain the same condition for $\omega_p = E_1^{(-)}$.

### 2. Condition of QDI-Induced PB without DDI

In the weak driving case (i.e., $\Omega_p \ll \kappa$), one can expand the system wave function to two-photon manifold with ansatz

$$|\Psi\rangle = \sum_{n=0}^{2} C_{gg,n}|gg,n\rangle + \sum_{n=1}^{2} C_{\pm,n-1}|\pm,n-1\rangle + C_{ee,n-2}|ee,n-2\rangle, \tag{A5}$$

where $|C_{\alpha_1\alpha_2,n}|^2$ represent the probabilities of occupation in state $|\alpha_1\alpha_2,n\rangle$ $(\{\alpha_1,\alpha_2\} = \{g,e\}, n = 0$–$2)$. Using the Schrödinger equation, the dynamical equations for the amplitudes $C_{\alpha_1\alpha_2,n}$ are given by

$$i\frac{\partial}{\partial t}C_{gg,1} = \left(-\Delta_c - \frac{i\kappa}{2}\right)C_{gg,1} + \sqrt{2}gC_{+,0} + \sqrt{2}\Omega_p C_{+,1}, \tag{A6a}$$

$$i\frac{\partial}{\partial t}C_{gg,2} = 2gC_{+,1} + (-2\Delta_c - i\kappa)C_{gg,2}, \tag{A6b}$$

$$H^{(n)} = \begin{pmatrix} n\omega_c & \sqrt{2n}g & 0 & 0 \\ \sqrt{2n}g & \omega_e + (n-1)\omega_c + J & 0 & \sqrt{2(n-1)}g \\ 0 & 0 & \omega_e + (n-1)\omega_c - J & 0 \\ 0 & \sqrt{2(n-1)}g & 0 & 2\omega_e + (n-2)\omega_c \end{pmatrix}. \tag{A9}$$

$$i\frac{\partial}{\partial t}C_{+,0} = \left(-\Delta_a - \frac{i\gamma}{2}\right)C_{+,0} + \sqrt{2}\Omega_p C_{gg,0} + \sqrt{2}gC_{gg,1} + \sqrt{2}\Omega_p C_{ee,0}, \tag{A6c}$$

$$i\frac{\partial}{\partial t}C_{+,1} = \left(-\Delta_a - \Delta_c - \frac{i\gamma}{2} - \frac{i\kappa}{2}\right)C_{+,1} + \sqrt{2}\Omega_p C_{gg,1} + 2gC_{gg,2} + \sqrt{2}gC_{ee,0}, \tag{A6d}$$

$$i\frac{\partial}{\partial t}C_{ee,0} = (-2\Delta_a - i\gamma)C_{ee,0} + \sqrt{2}\Omega_p C_{+,0} + \sqrt{2}gC_{+,1}. \tag{A6e}$$

Under the weak driving assumption, i.e., $C_{gg,0} \simeq 1 \gg C_{gg,1}, C_{+,0} \gg C_{gg,2}, C_{+,1}, C_{ee,0}$, one can easily obtain the steady-state solutions of the above equations, which yields

$$C_{gg,2} \approx -\frac{32\sqrt{2}ig^2\Omega_p^2(2\Delta_a + \Delta_c)}{F}, \tag{A7}$$

by assuming $\{\Delta_a, \Delta_c\} \gg \{\kappa, \gamma\}$, where $F = [\Delta_a(-4\Delta_c - 2i\kappa) - 2i\gamma\Delta_c + \gamma\kappa + 8g^2]\{-4\Delta_a^2(\kappa - 2i\Delta_c) - 2i\Delta_a[-4i\Delta_c(\gamma + \kappa) - 4\Delta_c^2 + 2\gamma\kappa + 8g^2 + \kappa^2] + \gamma^2\kappa - 4\gamma\Delta_c^2 - 2i\Delta_c(\gamma^2 + 2\gamma\kappa + 4g^2) + \gamma\kappa^2 + 8\gamma g^2 + 4g^2\kappa\}$.

Then, the realization of $g^{(2)}(0) \approx 2|C_{gg,2}|^2/|C_{gg,1}|^4 \to 0$ requires $C_{gg,2} = 0$, and one can easily obtain the condition of QDI-induced PB, i.e.,

$$\Delta_c = -2\Delta_a. \tag{A8}$$

In Fig. 7, we plot the equal-time second-order correlation function $g^{(2)}(0)$ [panel (a)] and mean photon number $\langle a^\dagger a\rangle$ [panel (b)] as functions of the atomic detuning $\Delta_c/\kappa$ and the cavity detuning $\Delta_a/\kappa$, respectively. Here, the dashed–dotted curves denote the condition of the ELA-based PB, and the dashed curves denote the condition of the QDI-induced PB. The system parameters are chosen as $\Omega_p = 0.1\kappa$, $g = 5\kappa$, and $\gamma = \kappa$. It is clear to see that the numerical results match the analytical solutions very well. Here, the dashed–dotted curves represent the condition of the ELA-based PB [i.e., Eq. (A4)], while the dashed line represents the condition of the QDI-induced PB [i.e., Eq. (A8)]. As shown in Fig. 7, although the value of $g^{(2)}(0)$ for the QDI-induced PB is much smaller than that for the ELA-based PB, the mean photon number is too small to be detected.

### 3. Condition of ELA-Based PB with DDI

In the presence of DDI, likewise, the Hamiltonian in $n$-photon space can be expressed as

Diagonalizing the above matrix, the eigenvalues and eigenstates in the one-photon space are given by

$$E_1^{(1)} = -J + \omega_a, \quad \text{with } \Psi_1^{(1)} = |-,0\rangle, \tag{A10a}$$

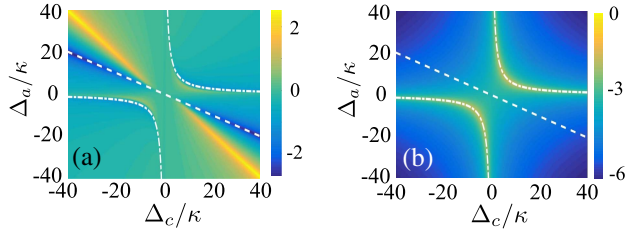


**Fig. 7.** Logarithmic plot of (a) the equal-time second-order correlation function $g^{(2)}(0)$ and (b) the mean photon number $\langle a^\dagger a\rangle$ as functions of the normalized atomic detuning $\Delta_c/\kappa$ and the cavity detuning $\Delta_a/\kappa$. The white dashed–dotted curves denote the condition of the ELA-based PB [i.e., Eq. (6)], and the white dashed lines denote the condition of the QDI-induced PB [i.e., Eq. (10)]. The system parameters are given by $\Omega_p = 0.1\kappa$, $g = 5\kappa$, and $\gamma = \kappa$.

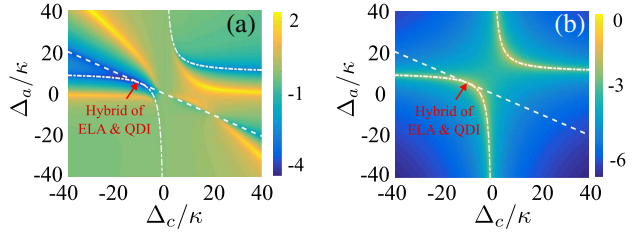


**Fig. 8.** Logarithmic plot of (a) the equal-time second-order correlation function $g^{(2)}(0)$ and (b) the mean photon number $\langle a^\dagger a\rangle$ as functions of $\Delta_c/\kappa$ and $\Delta_a/\kappa$ with $J = 2g$. The white dashed–dotted curves denote the condition of the ELA-based PB [i.e., Eq. (13)], and the white dashed lines denote the condition of the QDI-induced PB [i.e., $\Delta_c = -2\Delta_a$].

$$E_1^{(\pm)} = \frac{1}{2}\left[J+\omega_c+\omega_a \pm \sqrt{8g^2+(J+\omega_{ac})^2}\right] \text{ with}$$

$$\Psi_1^{(\pm)} = N_1^{(\pm)}\left[-\frac{J+\omega_{ac} \pm \sqrt{8g^2+(J+\omega_{ac})^2}}{2g}|gg,1\rangle + |+,0\rangle\right], \quad \textbf{(A10b)}$$

where $\omega_{ac} = \omega_a - \omega_c$ and $N_1^{\pm}$ are the normalization constants. It is noted that the product state $|-, n-1\rangle$ is also decoupled to other states of the system. The DDI only shifts the state $|\pm, n-1\rangle$ by the amount of $\pm J$, but does not affect other states. Thus, the condition of the ELA-based PB can be obtained by setting $\omega_p = E_1^+$ or $\omega_p = E_1^-$, which yields

$$g^2 = \frac{1}{2}\Delta_c(\Delta_a - J). \quad \textbf{(A11)}$$

It is noted that the condition of this ELA-based PB strongly depends on the DDI strength $J$. Therefore, one can adjust the DDI strength to coincide the conditions of the ELA-based and the QDI-induced PBs [indicated by the red arrows in Fig. 2] since the condition of the QDI-induced PB is insensitive to the DDI. As shown in Fig. 8, strong PB with large mean photon number can be achieved via the DDI.

**Funding.** National Key Basic Research Special Foundation (2016YFA0302800); National Natural Science Foundation of China (61975154, 11874287); Shanghai Science and Technology Committee (18JC1410900); Fundamental Research Funds of Shandong University.

**Acknowledgment.** We acknowledge the discussion with Prof. G. S. Agarwal at Texas A&M University.

**Disclosures.** The authors declare no conflicts of interest.

## REFERENCES AND NOTES

1. M. Lucamarini, Z. L. Yuan, J. F. Dynes, and A. J. Shields, "Overcoming the rate–distance limit of quantum key distribution without quantum repeaters," Nature **557**, 400–403 (2018).
2. N. Gisin, G. Ribordy, W. Tittel, and H. Zbinden, "Quantum cryptography," Rev. Mod. Phys. **74**, 145–195 (2002).
3. J. Volz, M. Weber, D. Schlenk, W. Rosenfeld, J. Vrana, K. Saucke, C. Kurtsiefer, and H. Weinfurter, "Observation of entanglement of a single photon with a trapped atom," Phys. Rev. Lett. **96**, 030404 (2006).
4. J. L. O'brien, "Optical quantum computing," Science **318**, 1567–1570 (2007).
5. M. Xiao, L.-A. Wu, and H. J. Kimble, "Precision measurement beyond the shot-noise limit," Phys. Rev. Lett. **59**, 278–281 (1987).
6. I. Kruse, K. Lange, J. Peise, B. Lücke, L. Pezzè, J. Arlt, W. Ertmer, C. Lisdat, L. Santos, A. Smerzi, and C. Klempt, "Improvement of an atomic clock using squeezed vacuum," Phys. Rev. Lett. **117**, 143004 (2016).
7. C. Lei, A. Weinstein, J. Suh, E. Wollman, A. Kronwald, F. Marquardt, A. Clerk, and K. Schwab, "Quantum nondemolition measurement of a quantum squeezed state beyond the 3 dB limit," Phys. Rev. Lett. **117**, 100801 (2016).
8. M. O. Scully and M. S. Zubairy, *Quantum Optics* (Cambridge University Press, 1999).
9. K. M. Birnbaum, A. Boca, R. Miller, A. D. Boozer, T. E. Northup, and H. J. Kimble, "Photon blockade in an optical cavity with one trapped atom," Nature **436**, 87–90 (2005).
10. A. Kuhn, M. Hennrich, and G. Rempe, "Deterministic single-photon source for distributed quantum networking," Phys. Rev. Lett. **89**, 067901 (2002).
11. A. Faraon, I. Fushman, D. Englund, N. Stoltz, P. Petroff, and J. Vučković, "Coherent generation of non-classical light on a chip via photon-induced tunnelling and blockade," Nat. Phys. **4**, 859–863 (2008).
12. A. Ridolfo, M. Leib, S. Savasta, and M. J. Hartmann, "Photon blockade in the ultrastrong coupling regime," Phys. Rev. Lett. **109**, 193602 (2012).
13. K. Müller, A. Rundquist, K. A. Fischer, T. Sarmiento, K. G. Lagoudakis, Y. A. Kelaita, C. Sánchez Muñoz, E. del Valle, F. P. Laussy, and J. Vučković, "Coherent generation of nonclassical light on chip via detuned photon blockade," Phys. Rev. Lett. **114**, 233601 (2015).
14. R. Sáez-Blázquez, J. Feist, F. J. Garca-Vidal, and A. I. Fernández-Domnguez, "Photon statistics in collective strong coupling: nanocavities and microcavities," Phys. Rev. A **98**, 013839 (2018).
15. C. Hamsen, K. N. Tolazzi, T. Wilk, and G. Rempe, "Two-photon blockade in an atom-driven cavity QED system," Phys. Rev. Lett. **118**, 133604 (2017).
16. C. J. Zhu, Y. P. Yang, and G. S. Agarwal, "Collective multiphoton blockade in cavity quantum electrodynamics," Phys. Rev. A **95**, 063842 (2017).
17. J. Z. Lin, K. Hou, C. J. Zhu, and Y. P. Yang, "Manipulation and improvement of multiphoton blockade in a cavity-QED system with two cascade three-level atoms," Phys. Rev. A **99**, 053850 (2019).
18. P. Rabl, "Photon blockade effect in optomechanical systems," Phys. Rev. Lett. **107**, 063601 (2011).
19. J.-Q. Liao and F. Nori, "Photon blockade in quadratically coupled optomechanical systems," Phys. Rev. A **88**, 023853 (2013).
20. H. Xie, C.-G. Liao, X. Shang, M.-Y. Ye, and X.-M. Lin, "Phonon blockade in a quadratically coupled optomechanical system," Phys. Rev. A **96**, 013861 (2017).
21. A. J. Hoffman, S. J. Srinivasan, S. Schmidt, L. Spietz, J. Aumentado, H. E. Türeci, and A. A. Houck, "Dispersive photon blockade in a superconducting circuit," Phys. Rev. Lett. **107**, 053602 (2011).
22. C. Lang, D. Bozyigit, C. Eichler, L. Steffen, J. M. Fink, A. A. Abdumalikov, M. Baur, S. Filipp, M. P. da Silva, A. Blais, and A. Wallraff, "Observation of resonant photon blockade at microwave frequencies using correlation function measurements," Phys. Rev. Lett. **106**, 243601 (2011).
23. Y.-X. Liu, X.-W. Xu, A. Miranowicz, and F. Nori, "From blockade to transparency: controllable photon transmission through a circuit-QED system," Phys. Rev. A **89**, 043818 (2014).
24. A. Miranowicz, M. Paprzycka, Y.-X. Liu, J. C. V. Bajer, and F. Nori, "Two-photon and three-photon blockades in driven nonlinear systems," Phys. Rev. A **87**, 023809 (2013).
25. G. Hovsepyan, A. Shahinyan, and G. Y. Kryuchkyan, "Multiphoton blockades in pulsed regimes beyond stationary limits," Phys. Rev. A **90**, 013839 (2014).
26. R. Huang, A. Miranowicz, J.-Q. Liao, F. Nori, and H. Jing, "Nonreciprocal photon blockade," Phys. Rev. Lett. **121**, 153601 (2018).
27. T. Liew and V. Savona, "Single photons from coupled quantum modes," Phys. Rev. Lett. **104**, 183601 (2010).
28. H. Flayac and V. Savona, "Unconventional photon blockade," Phys. Rev. A **96**, 053810 (2017).
29. H. Snijders, J. Frey, J. Norman, M. Bakker, E. Langman, A. Gossard, J. Bowers, M. Van Exter, D. Bouwmeester, and W. Löffler, "Purification of a single-photon nonlinearity," Nat. Commun. **7**, 12578 (2016).
30. J. Tang, W. Geng, and X. Xu, "Quantum interference induced photon blockade in a coupled single quantum dot-cavity system," Sci. Rep. **5**, 9252 (2015).
31. S. Ferretti, V. Savona, and D. Gerace, "Optimal antibunching in passive photonic devices based on coupled nonlinear resonators," New J. Phys. **15**, 025012 (2013).
32. H. Z. Shen, Y. H. Zhou, and X. X. Yi, "Tunable photon blockade in coupled semiconductor cavities," Phys. Rev. A **91**, 063808 (2015).

33. B. Sarma and A. K. Sarma, "Quantum-interference-assisted photon blockade in a cavity via parametric interactions," Phys. Rev. A **96**, 053827 (2017).
34. H. Wang, X. Gu, Y.-X. Liu, A. Miranowicz, and F. Nori, "Tunable photon blockade in a hybrid system consisting of an optomechanical device coupled to a two-level system," Phys. Rev. A **92**, 033806 (2015).
35. B. Li, R. Huang, X. Xu, A. Miranowicz, and H. Jing, "Nonreciprocal unconventional photon blockade in a spinning optomechanical system," Photon. Res. **7**, 630–641 (2019).
36. X.-W. Xu, A.-X. Chen, and Y.-X. Liu, "Phonon blockade in a nanomechanical resonator resonantly coupled to a qubit," Phys. Rev. A **94**, 063853 (2016).
37. H. Shen, C. Shang, Y. Zhou, and X. Yi, "Unconventional single-photon blockade in non-Markovian systems," Phys. Rev. A **98**, 023856 (2018).
38. M. Radulaski, K. A. Fischer, K. G. Lagoudakis, J. L. Zhang, and J. Vučković, "Photon blockade in two-emitter-cavity systems," Phys. Rev. A **96**, 011801 (2017).
39. M. Bamba, A. Imamoğlu, I. Carusotto, and C. Ciuti, "Origin of strong photon antibunching in weakly nonlinear photonic molecules," Phys. Rev. A **83**, 021802 (2011).
40. A. Majumdar, M. Bajcsy, A. Rundquist, and J. Vučković, "Loss-enabled sub-Poissonian light generation in a bimodal nanocavity," Phys. Rev. Lett. **108**, 183601 (2012).
41. X. Liang, Z. Duan, Q. Guo, C. Liu, S. Guan, and Y. Ren, "Antibunching effect of photons in a two-level emitter-cavity system," Phys. Rev. A **100**, 063834 (2019).
42. K. Hou, C. Zhu, Y. Yang, and G. Agarwal, "Interfering pathways for photon blockade in cavity QED with one and two qubits," Phys. Rev. A **100**, 063817 (2019).
43. C. Vaneph, A. Morvan, G. Aiello, M. Féchant, M. Aprili, J. Gabelli, and J. Estève, "Observation of the unconventional photon blockade in the microwave domain," Phys. Rev. Lett. **121**, 043602 (2018).
44. H. J. Snijders, J. A. Frey, J. Norman, H. Flayac, V. Savona, A. C. Gossard, J. E. Bowers, M. P. van Exter, D. Bouwmeester, and W. Löffler, "Observation of the unconventional photon blockade," Phys. Rev. Lett. **121**, 043601 (2018).
45. When a four-level atom with two closely spaced middle states is excited by four photons via different middle state (all one-photon excitation) such a system is often referred to as a diamond scheme four-wave mixing. For instance, the excitation of the D-state of an alkali atom simultaneously via $S\text{-}P_{1/2}\text{-}D$ and $S\text{-}P_{3/2}\text{-}D$ paths. If only three photons are provided this is the usual $2n\text{-}1$ excitation scheme in four-wave mixing; see also Ref. [46].
46. L. Deng, M. Payne, and W. Garrett, "Effects of multi-photon interferences from internally generated fields in strongly resonant systems," Phys. Rep. **429**, 123–242 (2006).
47. G. S. Agarwal, *Quantum Optics* (Cambridge University, 2013).
48. S. de Léséleuc, D. Barredo, V. Lienhard, A. Browaeys, and T. Lahaye, "Optical control of the resonant dipole-dipole interaction between Rydberg atoms," Phys. Rev. Lett. **119**, 053202 (2017).
49. D. Barredo, H. Labuhn, S. Ravets, T. Lahaye, A. Browaeys, and C. S. Adams, "Coherent excitation transfer in a spin chain of three Rydberg atoms," Phys. Rev. Lett. **114**, 113002 (2015).
50. K. Almutairi, R. Tanaś, and Z. Ficek, "Generating two-photon entangled states in a driven two-atom system," Phys. Rev. A **84**, 013831 (2011).
51. P. Lodahl, S. Mahmoodian, and S. Stobbe, "Interfacing single photons and single quantum dots with photonic nanostructures," Rev. Mod. Phys. **87**, 347–400 (2015).
52. H. Kim, D. Sridharan, T. C. Shen, G. S. Solomon, and E. Waks, "Strong coupling between two quantum dots and a photonic crystal cavity using magnetic field tuning," Opt. Express **19**, 2589–2598 (2011).
53. J.-H. Kim, S. Aghaeimeibodi, C. J. Richardson, R. P. Leavitt, and E. Waks, "Super-radiant emission from quantum dots in a nanophotonic waveguide," Nano Lett. **18**, 4734–4740 (2018).
54. J. Majer, J. Chow, J. Gambetta, J. Koch, B. Johnson, J. Schreier, L. Frunzio, D. Schuster, A. A. Houck, A. Wallraff, A. Blais, M. H. Devoret, S. M. Girvin, and R. J. Schoelkopf, "Coupling superconducting qubits via a cavity bus," Nature **449**, 443–447 (2007).
55. A. Grimm, F. Blanchet, R. Albert, J. Leppäkangas, S. Jebari, D. Hazra, F. Gustavo, J.-L. Thomassin, E. Dupont-Ferrier, F. Portier, and M. Hofheinz, "Bright on-demand source of antibunched microwave photons based on inelastic cooper pair tunneling," Phys. Rev. X **9**, 021016 (2019).
56. G. Sadiek, W. Al-Drees, and M. S. Abdallah, "Manipulating entanglement sudden death in two coupled two-level atoms interacting off-resonance with a radiation field: an exact treatment," Opt. Express **27**, 33799–33825 (2019).
57. O. Bitton, S. N. Gupta, and G. Haran, "Quantum dot plasmonics: from weak to strong coupling," Nanophotonics **8**, 559–575 (2019).
58. A. Browaeys, D. Barredo, and T. Lahaye, "Experimental investigations of dipole–dipole interactions between a few Rydberg atoms," J. Phys. B **49**, 152001 (2016).
59. E. Urban, T. A. Johnson, T. Henage, L. Isenhower, D. Yavuz, T. Walker, and M. Saffman, "Observation of Rydberg blockade between two atoms," Nat. Phys. **5**, 110–114 (2009).
60. T. A. Johnson, E. Urban, T. Henage, L. Isenhower, D. Yavuz, T. Walker, and M. Saffman, "Rabi oscillations between ground and Rydberg states with dipole-dipole atomic interactions," Phys. Rev. Lett. **100**, 113003 (2008).
61. R. Reimann, W. Alt, T. Kampschulte, T. Macha, L. Ratschbacher, N. Thau, S. Yoon, and D. Meschede, "Cavity-modified collective Rayleigh scattering of two atoms," Phys. Rev. Lett. **114**, 023601 (2015).
62. M. Bayer, P. Hawrylak, K. Hinzer, S. Fafard, M. Korkusinski, Z. Wasilewski, O. Stern, and A. Forchel, "Coupling and entangling of quantum states in quantum dot molecules," Science **291**, 451–453 (2001).
63. J. D. Cox, M. R. Singh, G. Gumbs, M. A. Anton, and F. Carreno, "Dipole-dipole interaction between a quantum dot and a graphene nanodisk," Phys. Rev. B **86**, 125452 (2012).
64. M. Saffman and T. Walker, "Analysis of a quantum logic device based on dipole-dipole interactions of optically trapped Rydberg atoms," Phys. Rev. A **72**, 022347 (2005).
65. B. T. Gard, K. Jacobs, R. McDermott, and M. Saffman, "Microwave-to-optical frequency conversion using a cesium atom coupled to a superconducting resonator," Phys. Rev. A **96**, 013833 (2017).
66. F. Quijandra, U. Naether, S. K. Özdemir, F. Nori, and D. Zueco, "PT-symmetric circuit QED," Phys. Rev. A **97**, 053846 (2018).